JOURNAL OF SYNCHROTRON RADIATION

Volume 26 (2019)

Supporting information for article:

A beamline-compatible STED microscope for combined visible-light and X-ray studies of biological matter

Marten Bernhardt, Jan-David Nicolas, Markus Osterhoff, Haugen Mittelstädt, Matthias Reuss, Benjamin Harke, Andrew Wittmeier, Michael Sprung, Sarah Köster and Tim Salditt

Supporting information for article:

A beamline-compatible STED microscope for combined visible light and x-ray studies of biological matter

M. Bernhardt[1], J.-D. Nicolas[1], M. Osterhoff[1], H. Mittelstädt[2], M. Reuss[2], B. Harke[2], A. Wittmeier[1], M. Sprung[3], S. Köster[1], T. Salditt[1,*]

[1]Institut für Röntgenphysik, Universität Göttingen, Friedrich-Hund-Platz 1, Göttingen D-37077, Germany.

[2]Abberior Instruments, Hans-Adolf-Krebs-Weg 1, Göttingen D-37077, Germany.

[3]Deutsches Elektronen-Synchrotron (DESY), Notkestraße 47c, Hamburg D-22607, Germany.

S1. Instrumentation, equipment and transport

All optical components of the microscope are mounted on two separate optical breadboards, as described in Sec. 2 and Sec. 3 of the main article. The microscope consists of a *laser and detector box* (approximate size: $45 \times 13 \times 40\,\mathrm{cm}^3$, width $\times$ height $\times$ depth) comprising the lasers, the safety shutters as well as the detector, and an *optics box* (approximate size including objective: $25 \times 58 \times 23\,\mathrm{cm}^3$; approximate size including objective and top-view camera: $25 \times 80 \times 28\,\mathrm{cm}^3$) which includes all further optical components such as the "easySTED" unit and the entire full-field epifluorescence microscope. Figure S1(a) shows a front-view photograph of the computer rack. The control computer, power supplies, different controllers for the lasers and AOMs as well as the *laser and detector box* are stacked on top of each other. In order to avoid significant misalignment of the optical components during transport, the rack is mounted on a small cart. The cart also includes a framework for the *optics box*, which can be placed in the back, see Fig. S1(b-c). The entire cart (approximate size: $75 \times 110 \times 130\,\mathrm{cm}^3$) can be lifted into the trunk of a van, see Fig. S1(d, red frame), *e.g.* for transportation to the DESY campus. A light-protective desiccator and a mobile incubator are available to transport fluorescently labeled freeze-dried, chemically fixated and alive samples, see Fig. S1(d, blue and green frame). The incubator can be powered by the car battery and the temperature can be set to $277\,\mathrm{K}$ for chemically fixated samples and to $310\,\mathrm{K}$ for samples in the living state.
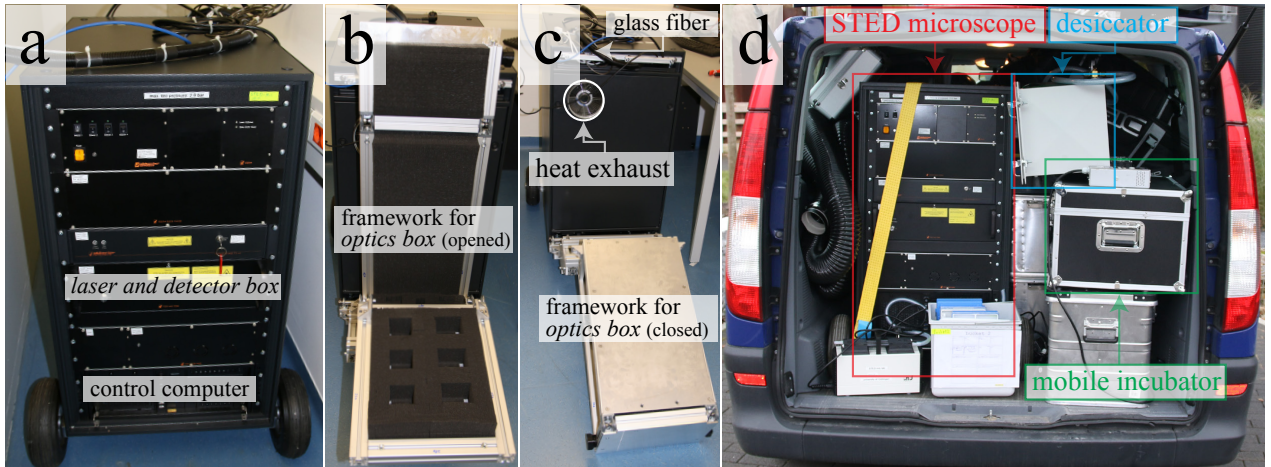

Figure S1: (a-d) Photographs of the STED microscope mounted on a mobile cart in the lab, see (a-c), and lifted in the trunk of a van ready for transport, see (d).

Figure S2 illustrates the setup after installation at the beamline. Figure S2(a-c) shows the GINIX-instrument in different working modes. Figure S2(a): Freeze-dried cardiac tissue cells (white film) adhering to a glass substrate are positioned in the focal plane of the STED objective. The luminescent red dot originates from the attenuated epifluorescence illumination in full-field mode of the microscope. Figure S2(b) shows a photograph along the y-direction with the STED beam axis in front, and the x-ray beam axis further in the back. In this photograph, the sample tower is placed at an x-ray recording position with the sample being inspected by the OAV in reflection mode, see white luminescent LED-ring. The OAV (working distance: $5\,\mathrm{cm}$) is directed towards the beam source, see Fig. S2(c), and enables monitoring of the sample during the x-ray recordings. The sample is placed in a defocus position of an x-ray waveguide for holography. Figure S2(d) shows the recent, upgraded setup including a new hexapod sample tower. Top- and side-view cameras are now available to monitor the distance between the sample and STED objective, facilitating tilt alignment with respect to the focal plane of the microscope, see Fig. S2(e-f).

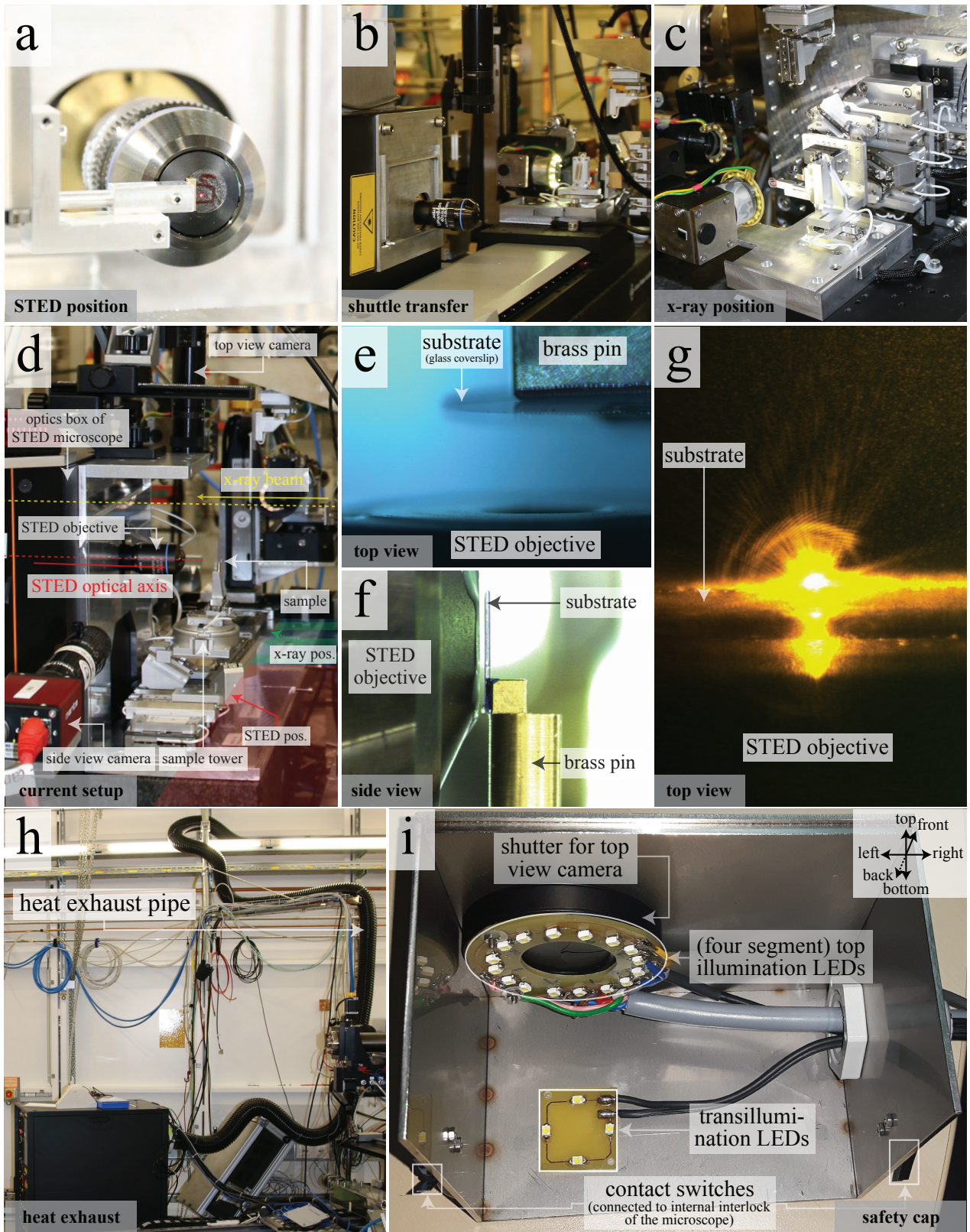*Corresponding author, Tel.: (+49)551-399427, e-mail: tsaldit@gwdg.de

Figure S2: (*a-c*) Photographs of the combined STED and x-ray microscope in different working modes. Adapted from (Bernhardt *et al.*, 2018). (*d*) Current version of the combined setup including the new hexapod sample tower with its long translation rail. Top- and side view cameras are now permanently available to monitor the distance between the sample and the STED objective as well as possible tilts of the sample from two different angles, which can then be corrected exploiting the rotational degrees of freedom of the hexapod. Adapted from (Bernhardt *et al.*, 2018). (*e-f*) Top and side view of samples approaching the STED objective. (*g*) Top view during a STED recording. (*h*) Photograph of the computer rack with an installed heat exhaust pipe. (*i*) Safety cap including the iris-shutter for top-view monitoring, a segmented top LED illumination ring and the transillumination LEDs in the back.

Figure S2(*g*) shows a micrograph of the top view camera with the STED pulse impinging on a (glass)

substrate. The microscope is equipped with a 10 m heat exhaust pipe, which can be connected to the computer rack in order to directly transfer the heat out of the hutch, thus avoiding uncontrolled thermal drifts of the GINIX nano-positioning motors, see Fig. S2(h). Figure S2(i) shows the safety cap, which is placed on top of the sample tower before a STED recording. It includes an LED ring top illumination and an LED transillumination for bright field microscopy. The different LED segments are separately connected to a patch panel inside the computer rack and can be triggered by the STED control software ("Imspector", Abberior Instruments). An iris-shutter under the top is necessary for monitoring the working distance and can be closed before performing a STED recording thus protecting the camera from the STED laser. Two contact switches positioned at the sides are fed back to the internal interlock system, so that the microscope can be operated as a standalone instrument without the need of an external beamline interlock system. For specifications of the excitation and STED laser as well as the epifluorescence LED, see Tab. S1.

Excitation laser		STED laser		Epifluorescence LED	
laser class	3B	laser class	4	risk group:	RG0
wavelength:	(632 ± 4) nm (pulsed)	wavelength:	(775 ± 1.5) nm	nominal wavelength:	625 nm
	(639 ± 1) nm (cw)			bandwidth (FWHM):	18 nm
max. Repetition rate:	80 MHz	max. repetition rate:	25-45 MHz	LED output power:	770 mW
operating mode:	pulsed/cw	operating mode:	pulsed		
output power:	12 mW	max. energy per pulse:	>30 nJ		
pulse length:	≈ 33 ps	pulse duration:	1.3 ns		
power consumption:	<20 W	jitter:	<100 ps		
		max. average power:	1.25 W @ 40 MHz		

Table S1: Specifications of the excitation laser, the STED laser and the epifluorescence LED.

The beam diameter in the focus of the KB mirrors is determined by successive translation of a waveguide through the focal plane. At each scan position, the overall intensity as recorded by the 2D panel of a single-photon counting detector (Pilatus 300 K, Dectris) is integrated, yielding the curves shown in Fig. S3(a-b, blue crosses) for the horizontal and vertical direction, respectively. Data points were fitted by a Gaussian function (red lines). The beam sizes are roughly around $300 \times 300\,\text{nm}^2$ (horizontal$\times$vertical), as derived from the FWHM-values (green lines), and are depending on fit quality and experimental parameters. The KB photon flux $I_0 = 1.11 \cdot 10^{11}$ photons/s was determined by recording the attenuated primary beam with the pixel detector (Pilatus 300 K, Dectris), see Fig. S3(c).
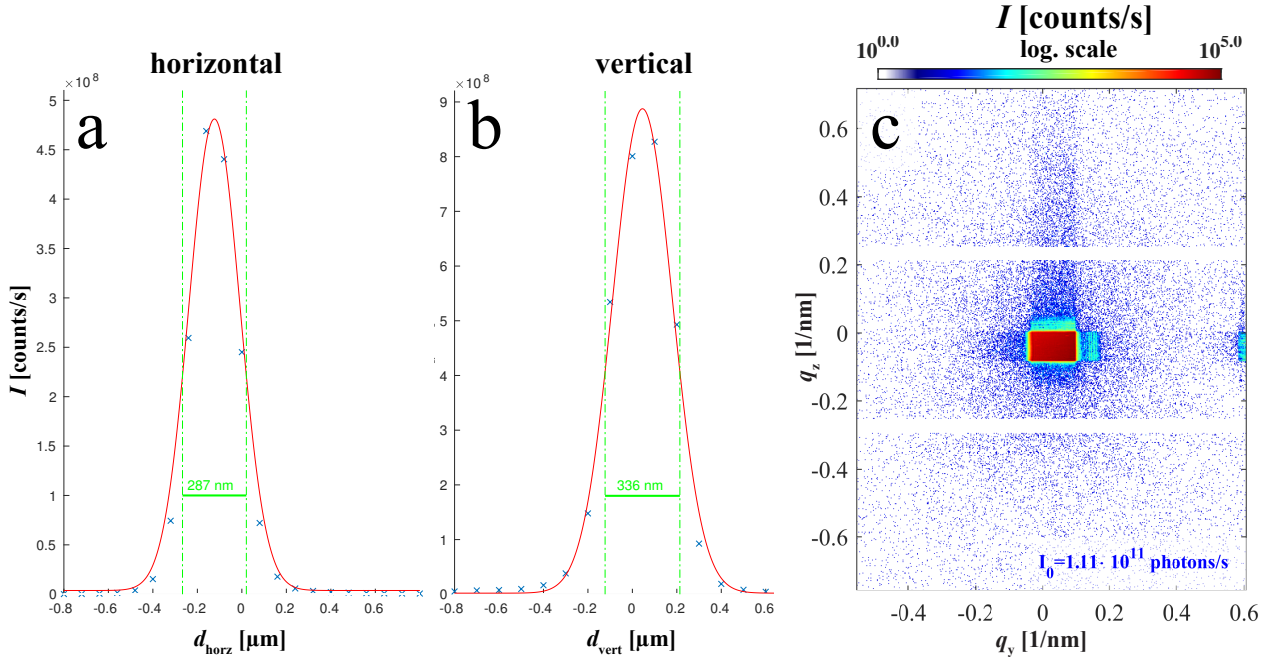

Figure S3: (a-b) Horizontal and vertical beam diameter as determined from translating a waveguide through the KB focus. The 2D patterns of the detector were integrated for each scan position (blue crosses) and full-width half maximum (FWHM) values of a Gaussian function (red lines) were computed and are shown in green. (c) Far-field of the attenuated primary beam. After correcting for the attenuators (Molybdenum-foils), the beam flux is determined to $I_0 = 1.11 \cdot 10^{11}$ photons/s.

Several upgrades of the STED microscope are possible in order to facilitate the alignment procedure of the internal optical components, and to achieve a more compact and flexible design. In this way the microscope can be turned into a fully equipped lab instrument, whenever it is not installed at the beamline. As shorter-term upgrades, the safety cap will be motorized in order to facilitate lab- and beamline use and the microscope design will be compacted by permanently installing the top- and side-view camera on an adapter plate at the

top of the *optics box*, see Fig. S4. Furthermore, we plan to motorize essential mirrors, which would enable a remote alignment of the microscope without the need of opening any housing. Another upgrade would be to mount the *optics box* on an arm as shown in Fig. S4 thus enabling rotation. With the *optics box* aligned in the horizontal direction, hydrated samples in standard petri dishes could be investigated just like with any other inverted-style lab microscope.
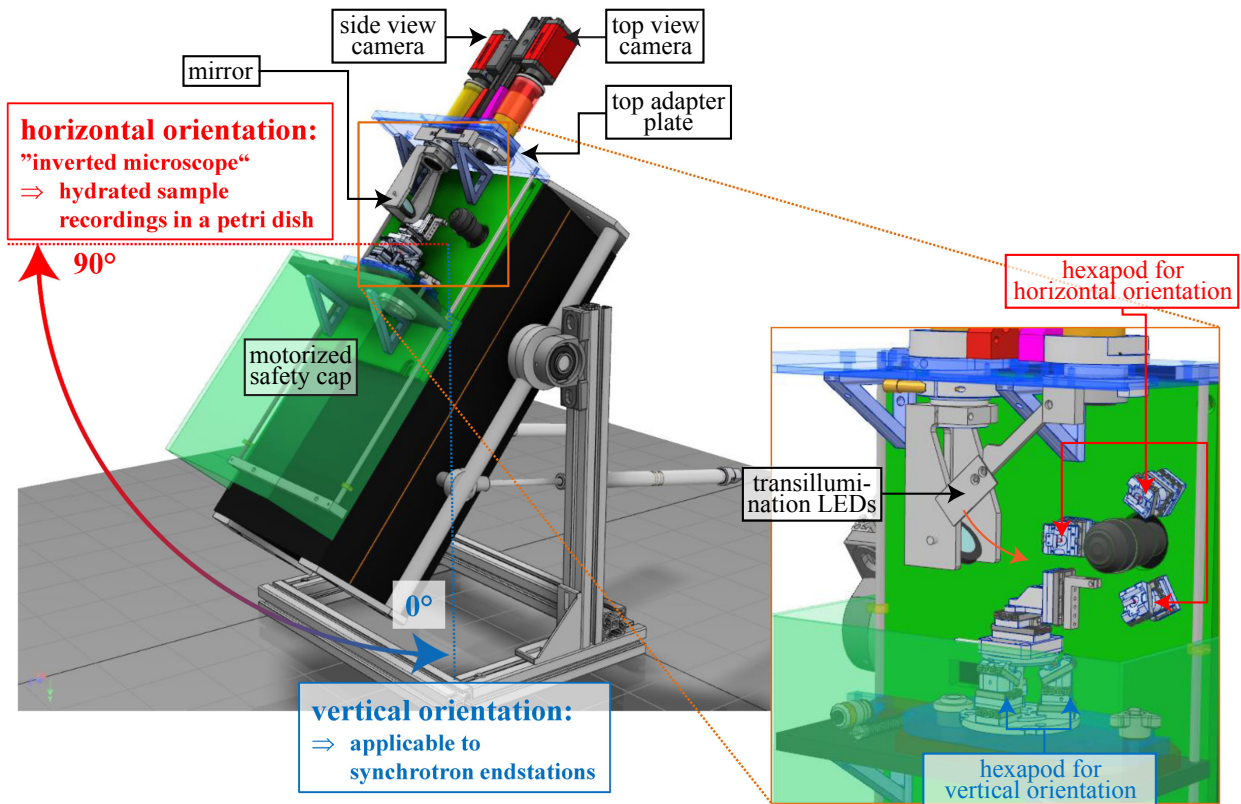

Figure S4: Possible upgrades towards using the STED microscope as a fully equipped lab source, facilitating handling and alignment procedures and converting the instrument into an inverted microscope by flipping the *optics box* into the horizontal direction. When flipped, the instrument is now also being able to probe liquid-covered, hydrated samples in a petri dish.

S2. Sample recording, workflow and additional results

A typical workflow for an *in situ* STED recording of a particular sample ROI requires all four imaging modalities of the STED microscope: Bright field and epifluorescene imaging in full-field mode are followed by confocal and STED imaging in scanning mode. Figure S5 shows a stitched, gray-colored DIC micrograph of an entire glass-substrate window as recorded by a "conventional" lab microscope (Zeiss Observer Z1) before the synchrotron recording campaign. At

ROI	Figure no.
①	▷Fig. 4; ▷Fig. S9; ▷Fig. S10
②	▷Fig. 5; ▷Fig. S8; ▷Fig. S11
③	▷Fig. S7; ▷ref. (Bernhardt *et al.*, 2018), Fig. 2-3
④	▷ref. (Bernhardt *et al.*, 2018), Fig. 1

Table S2: Sample ROIs and their assignment to the presented figures in this and our preceding manuscript, see (Bernhardt *et al.*, 2018).
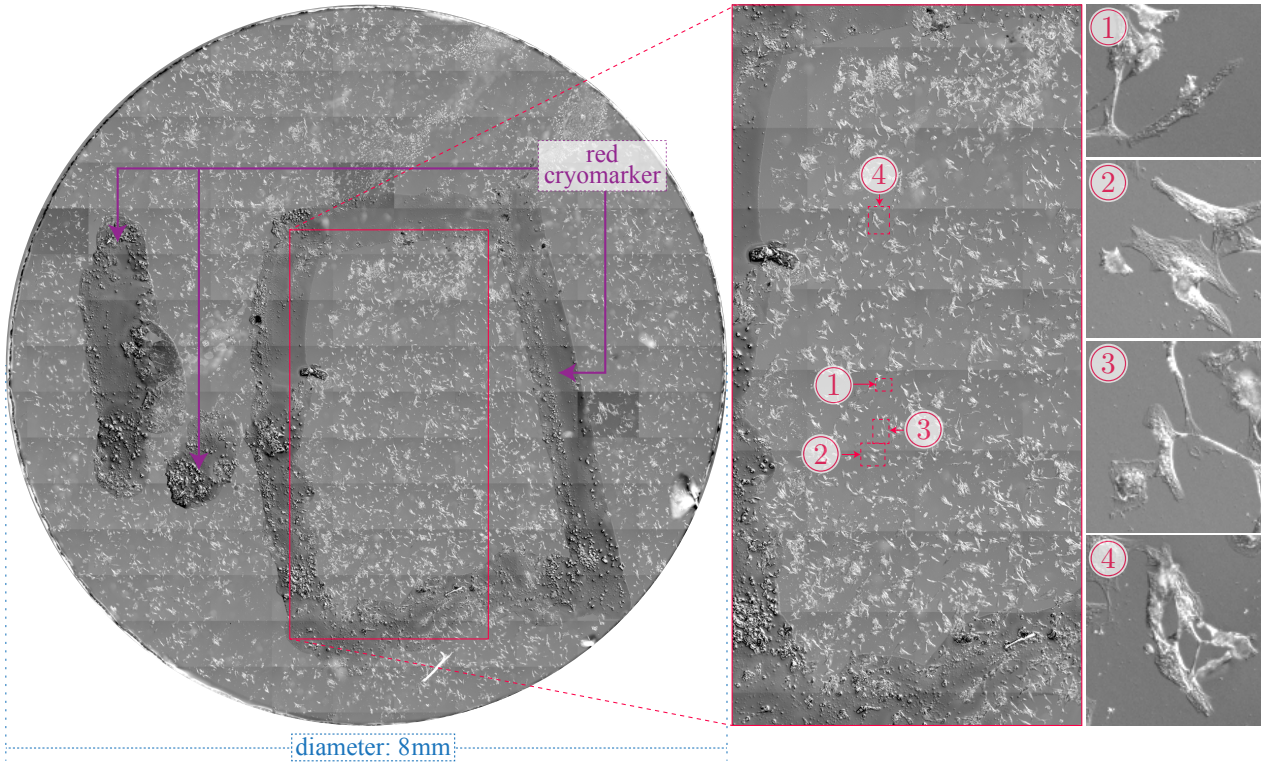
the beamline, the overview stitch was used for navigation on the sample in order to find particular sample ROIs. Annotated cells correspond to the different sample ROIs as presented in this manuscript and in our preceding work of (Bernhardt *et al.*, 2018), see Tab. S2. Dark marker lines of the image originate from a red cryomarker in order to improve orientation on the sample plane. At the beamline, the STED microscope is first used in bright field mode for a quick overview, which enables to identify the current position irrespective of any fluorescent labeling, see Fig. S6(a). Next, the quality of the fluorescence signal can be judged very quickly by applying the "live" (full-field) epifluorescence mode, see Fig. S6(b). Especially for time-resolved imaging the epifluorescence mode can be particularly useful before recording confocal or STED scans on small sample areas. When a suitable cell is found, a coarse confocal overview scan is used to review the cell in confocal mode. The piezo stage of the objective scanner allows translations along all three axes, which can be used for focusing the sample. This is followed by a combined confocal and STED scan of the area. Figure S6(c-d) shows an example of a "final" combined confocal and STED scan. Figure S7 shows a coarse overview confocal scan together with a line scan along the optical axis in order to find the correct focal plane.

The maximum FOV for the $40\times$ objective in full-field mode is approximately $130\,\mu m \times 175\,\mu m$. In scanning mode, the FOV is limited by the travel range of the piezo scanner, which at the current stage is $100\,\mu m$ at most. Figure S8 relates the maximum FOVs in both recording modes to a typical size of an adherent NRCTC as imaged by differential interference contrast (DIC) microscopy.

Figure S5: $10\times$ DIC overview of the freeze-dried sample before any STED or x-ray recording. Different sample ROIs denoted as area ①-④ correspond to the results shown here and in the main article as well as in our preceding work (Bernhardt *et al.*, 2018).
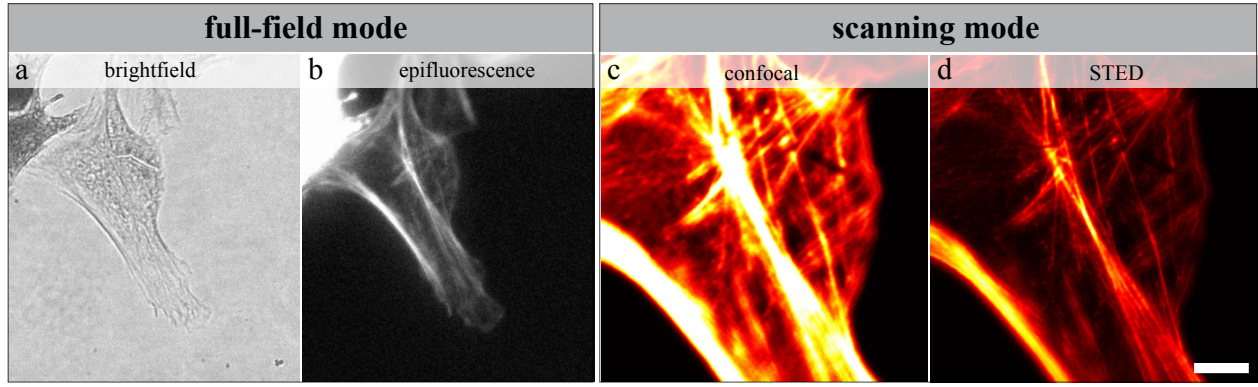
Figure S6: Micrographs of a single cardiac tissue cells in all four imaging modes of the STED microscope. Bright field and epifluorescence micrographs are acquired in full-field, and the confocal and STED micrographs are recorded in scanning mode. Scale bar: 5 µm.
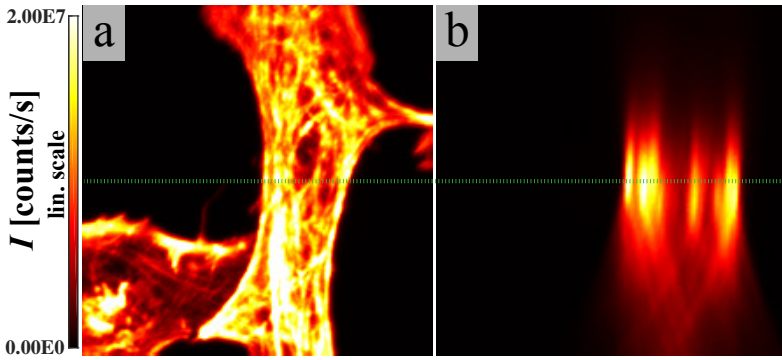

Figure S7: (a-b) Scan of a NRCTC in yz- and xy-direction, respectively. A dotted green line indicates the line scan position in the yz-scan and the central position in the xy-scan.
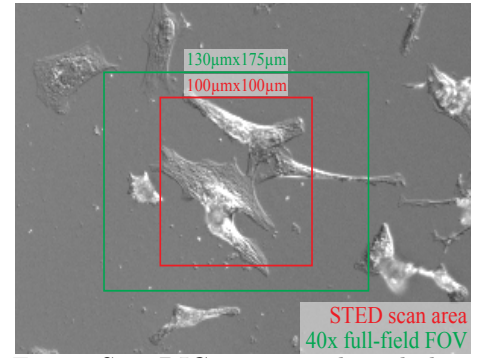
Figure S8: DIC micrograph including the FOV for full-field mode (green) and maximum scan area in scanning mode (red) of the STED microscope.
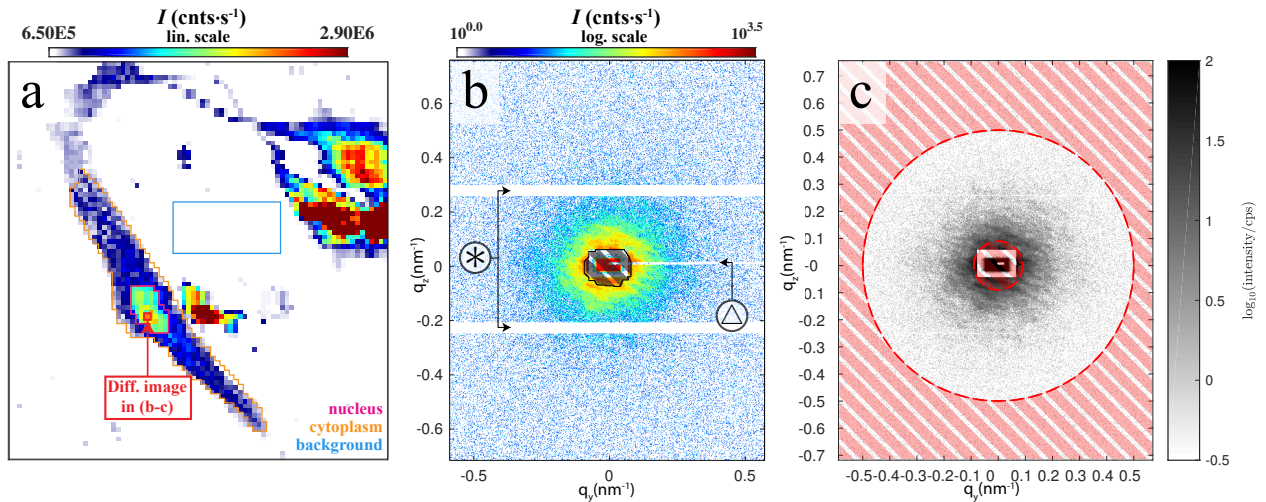

Figure S9: (a) X-ray darkfield image of a freeze-dried NRCTC, enabling to distinguish nucleic-, cytoplasmic- and background-related signals. (b) Single diffraction pattern corresponding to the position marked in (a). The hatched region indicates the binary mask applied for x-ray darkfield analysis. (c) Processed diffraction image after subtracting an average background signal and using the "heal" function of the nanodiffraction toolbox (Nicolas, 2017; Nicolas et al., 2017). PCA was applied on such processed images after cropping data with a radial-symmetric binary mask (red hatched/non-hatched region).

For x-ray darkfield and PCA evaluation of diffraction data, we have defined two different binary masks, masking out parasitic scattering tails caused by KB-focusing as well as the primary beam itself. Figure S9(a) reviews the x-ray darkfield image of Fig. 4 (main article). Figure S9(b) shows a diffraction pattern of the nucleus

as marked in (*a*, red frame) together with the applied x-ray darkfield mask (hatched black region). For PCA, an average background signal was subtracted, as previously defined by a STXM mask on the x-ray darkfield (see *a*, blue frame), and we have processed the diffraction data using the "heal" function of the nanodiffraction toolbox (Nicolas, 2017; Nicolas *et al.*, 2017). The function fills in missing data of the intermodular gaps of the Pilatus 300 K detector, (*b*, area ✳) as well as of the non-transparent beamstop holder (*b*, area △) by symmetry. Finally, a binary radial-symmetric mask was applied, see (*c*, red hatched/non-hatched region), defining the area which was then evaluated by PCA.

   Figure S10 and Fig. S11 show diffraction data of the areas presented in Fig. 4 and Fig. 5(main article) as composites. All patterns have been background-subtracted and healed as described above, using the average background signal of the areas as defined in Fig. S9(*a*) and in Fig. S11(inset). The data shown are restricted to the central detector area around the beamstop.
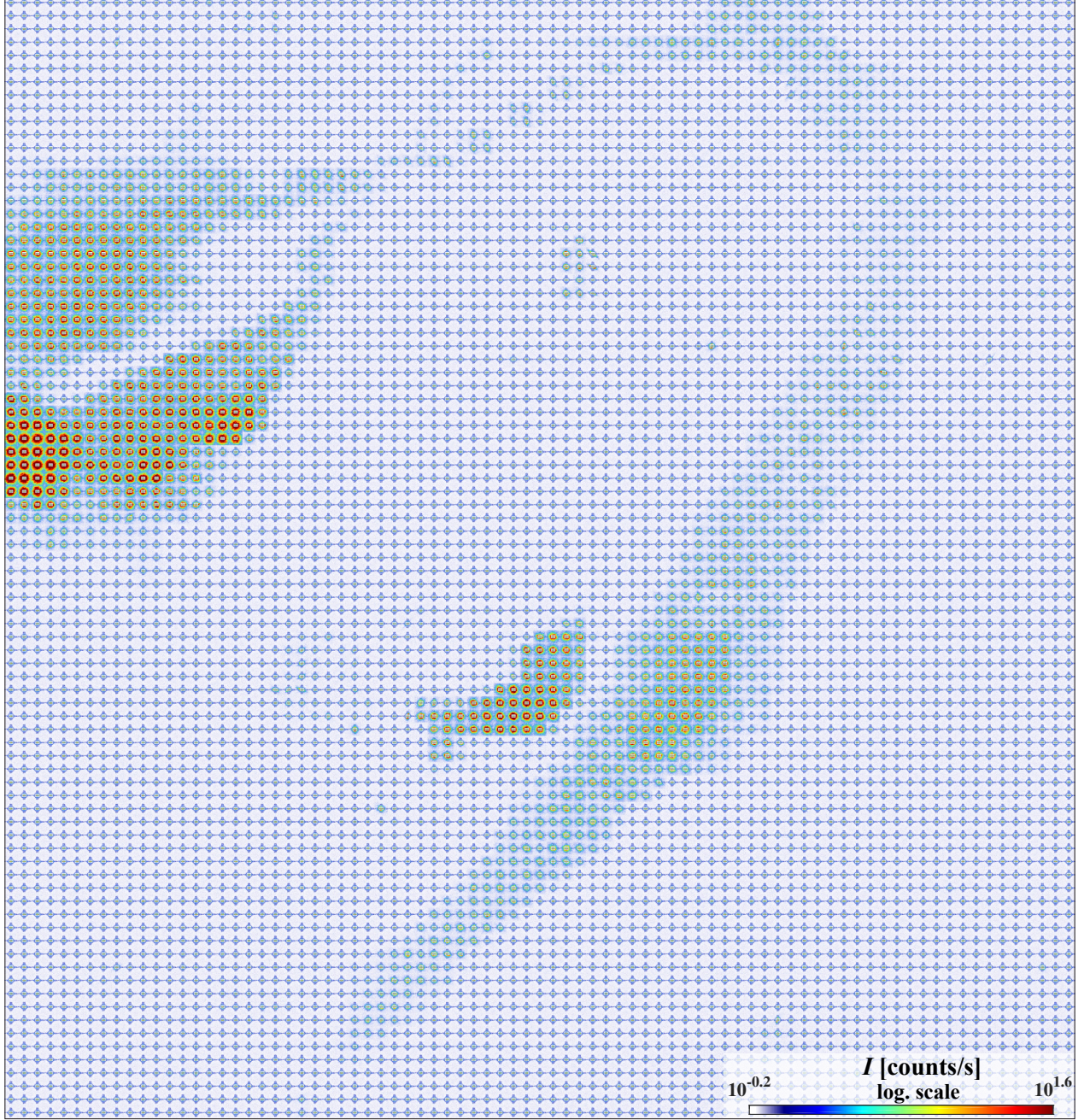

Figure S10: Composite image of the sample ROI shown in Fig. 4 of the main article. Diffraction patterns were cropped around the primary beam position, background-corrected using the average background signal as defined in Fig. S9(*a*) and healed.
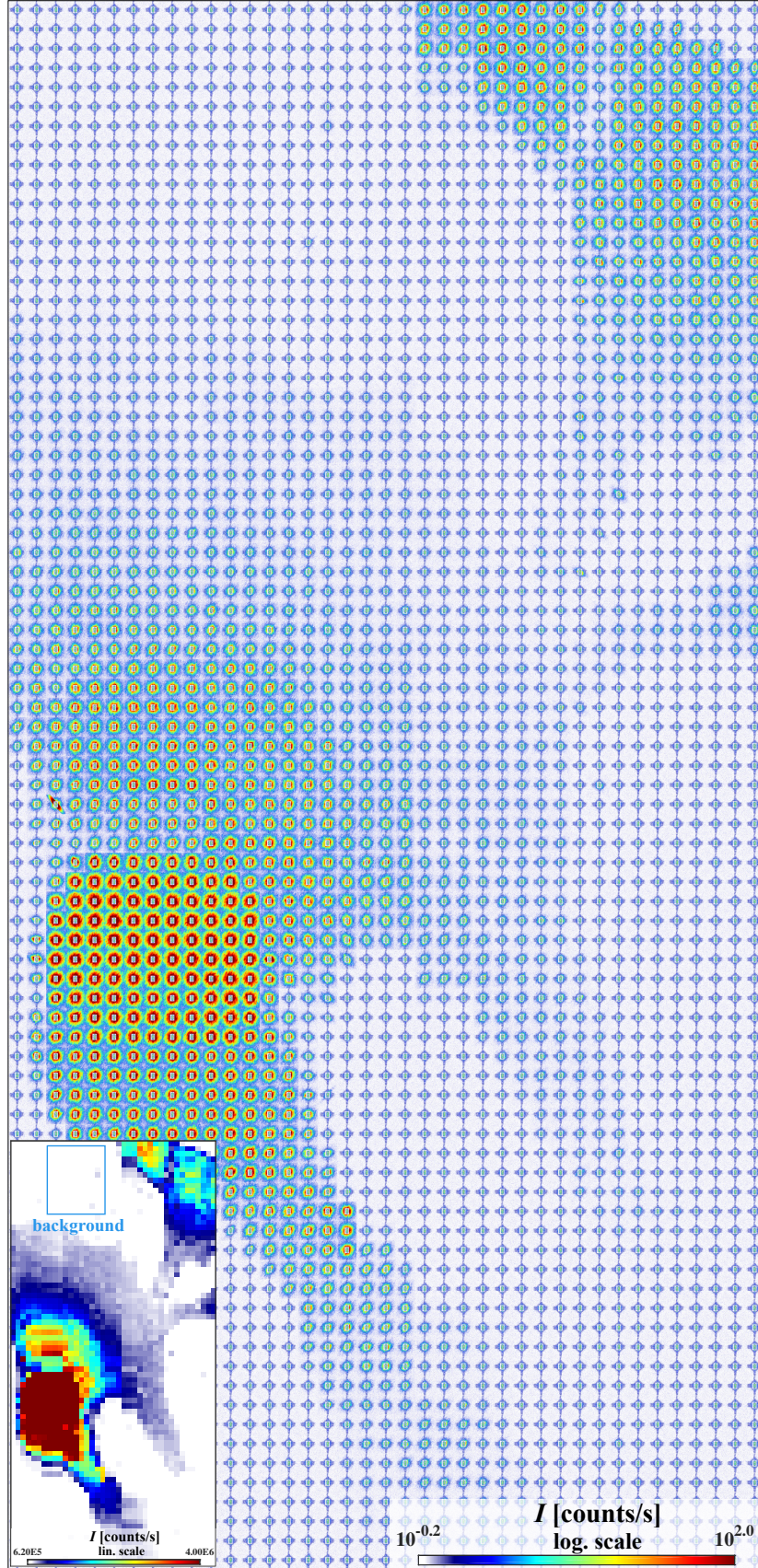
Figure S11: Composite image of the sample ROI shown in Fig. 5 of the main article. Diffraction patterns were cropped around the primary beam position, background-corrected using the average background signal as defined on the x-ray darkfield, see inset (blue box) and healed.

References

Bernhardt, M., J.-D. Nicolas, M. Osterhoff, H. Mittelstädt, M. Reuss, B. Harke, A. Wittmeier, M. Sprung, S. Köster, & T. Salditt (2018). "Correlative microscopy approach for biology using X-ray holography, X-ray scanning diffraction and STED microscopy". In: *Nature Communications* 9.1, p. 3641.

Nicolas, J.-D. (2017). *https://irpgoe.github.io/nanodiffraction/*.

Nicolas, J.-D., M. Bernhardt, A. Markus, F. Alves, M. Burghammer, & T. Salditt (2017). "Scanning x-ray diffraction on cardiac tissue: automatized data analysis and processing". In: *Journal of Synchrotron Radiation* 24.6, pp. 1163–1172.